J|A|C|S
ARTICLES
Published on Web 08/17/2002

An NMR Experiment for the Accurate Measurement of Heteronuclear Spin-Lock Relaxation Rates

Dmitry M. Korzhnev,[†] Nikolai R. Skrynnikov,[†] Oscar Millet,[†] Dennis A. Torchia,[‡] and Lewis E. Kay*[,†]

Contribution from the Protein Engineering Network Centers of Excellence and Departments of Medical Genetics, Biochemistry and Chemistry, University of Toronto, Toronto, Ontario M5S 1A8, Canada, and Molecular Structural Biology Unit, National Institute of Dental and Craniofacial Research, National Institutes of Health, Bethesda, Maryland 20892

Received April 2, 2002. Revised Manuscript Received June 7, 2002

Abstract: Rotating-frame relaxation rates, $R_{1\rho}$, are often measured in NMR studies of protein dynamics. We show here that large systematic errors can be introduced into measured values of heteronuclear $R_{1\rho}$ rates using schemes which are usually employed to suppress cross-correlation between dipole−dipole and CSA relaxation mechanisms. For example, in a scalar-coupled two-spin X−H spin system the use of ^{1}H WALTZ16 decoupling or ^{1}H pulses applied at regularly spaced intervals leads to a significant overestimation of heteronuclear $R_{1\rho}$ values. The problem is studied experimentally and theoretically for ^{15}N−^{1}H and ^{13}C−^{1}H spin pairs, and simple schemes are described which eliminate the artifacts. The approaches suggested are essential replacements of existing methodology if accurate dynamics parameters are to be extracted from spin-lock relaxation data sets.

Introduction

Heteronuclear NMR spin-relaxation measurements provide a powerful tool to probe conformational dynamics in macromolecules.[1−4] ^{15}N relaxation methods are now routine for studying backbone mobility in proteins [1,3] and have been supplemented in the past few years by new ^{13}C and ^{2}H relaxation techniques, allowing direct probes of protein side-chain dynamics.[5−14] Many relaxation experiments rely on the application of on- or off-resonance radio frequency (rf) fields which lock magnetization along the effective field in the rotating frame.[15] On-resonance rotating frame relaxation experiments have been used routinely to estimate transverse relaxation rates, R_2, for the analysis of pico- to nanosecond time-scale dynamics in proteins.[16] Off-resonance experiments, in turn, have been employed to quantify micro- to millisecond time scale conformational exchange in macromolecules.[17−21] Recent theoretical developments suggest that rotating-frame experiments are likely to be extremely useful in characterizing exchange processes that are outside the fast-exchange limit.[22]

The accurate description of protein dynamics by NMR is predicated on the use of robust experimental methods that are free of any systematic errors. Uncertainties in heteronuclear autorelaxation rates on the order of 1−2% are usually obtained from exponential fitting of signal intensities in a series of relaxation spectra or in repeated measurements.[1] This is, however, a very optimistic estimate if one considers the potential systematic errors that may be inherent to a particular experiment or that may be introduced due to hardware imperfections. For example, heteronuclear R_2 values derived from $R_{1\rho}$ measurements can be affected by poor alignment of magnetization along the effective field,[20] miscalibration of the spin-lock field strength

* To whom correspondence should be addressed. E-mail: kay@pound.med.utoronto.ca.
[†] University of Toronto.
[‡] National Institutes of Health.

(1) Korzhnev, D. M.; Billeter, M.; Arseniev, A. S.; Orekhov, V. Y. *Prog. Nucl. Magn. Reson. Spectrosc.* **2001**, *38*, 197−266.
(2) Kay, L. E. *Nat. Struct. Biol.* **1998**, *5*, 513−517.
(3) Palmer, A. G.; Williams, J.; McDermott, A. *J. Phys. Chem.* **1996**, *100*, 13293−13310.
(4) Ishima, R.; Torchia, D. A. *Nat. Struct. Biol.* **2000**, *7*, 740−743.
(5) Nicholson, L. K.; Kay, L. E.; Baldisseri, D. M.; Arango, J.; Young, P. E.; Bax, A.; Torchia, D. A. *Biochemistry* **1992**, *31*, 5253−5263.
(6) Muhandiram, D. R.; Yamazaki, T.; Sykes, B. D.; Kay, L. E. *J. Am. Chem. Soc.* **1995**, *117*, 11536−11544.
(7) Pervushin, K.; Wider, G.; Wuthrich, K. *J. Am. Chem. Soc.* **1997**, *119*, 3842−3843.
(8) Yang, D. W.; Mittermaier, A.; Mok, Y. K.; Kay, L. E. *J. Mol. Biol.* **1998**, *276*, 939−954.
(9) LeMaster, D. M.; Kushlan, D. M. *J. Am. Chem. Soc.* **1996**, *118*, 9255−9264.
(10) Wand, A. J.; Urbauer, J. L.; McEvoy, R. P.; Bieber, R. J. *Biochemistry* **1996**, *35*, 6116−6125.
(11) Mulder, F. A. A.; Skrynnikov, N. R.; Hon, B.; Dahlquist, F. W.; Kay, L. E. *J. Am. Chem. Soc.* **2001**, *123*, 967−975.
(12) Skrynnikov, N. R.; Mulder, F. A. A.; Hon, B.; Dahlquist, F. W.; Kay, L. E. *J. Am. Chem. Soc.* **2001**, *123*, 4556−4566.
(13) Millet, O.; Muhandiram, D. R.; Skrynnikov, N. R.; Kay, L. E. *J. Am. Chem. Soc.* **2002**, *124*, 6439−6448.
(14) Ishima, R.; Petkova, A. P.; Louis, J. M.; Torchia, D. A. *J. Am. Chem. Soc.* **2001**, *123*, 6164−6171.
(15) Desvaux, H.; Berthault, P. *Prog. Nucl. Magn. Reson. Spectrosc.* **1999**, *35*, 295−340.
(16) Peng, J. W.; Thanabal, V.; Wagner, G. *J. Magn. Reson.* **1991**, *94*, 82−100.
(17) Palmer, A. G.; Kroenke, C. D.; Loria, J. P. *Methods Enzymol.* **2001**, *339*, 204−238.
(18) Akke, M.; Palmer, A. G. *J. Am. Chem. Soc.* **1996**, *118*, 911−912.
(19) Zinn-Justin, S.; Berthault, P.; Guenneugues, M.; Desvaux, H. *J. Biomol. NMR* **1997**, *10*, 363−372.
(20) Mulder, F. A. A.; de Graaf, R. A.; Kaptein, R.; Boelens, R. *J. Magn. Reson.* **1998**, *131*, 351−357.
(21) Hoogstraten, C. G.; Wank, J. R.; Pardi, A. *Biochemistry* **2000**, *39*, 9951−9958.
(22) Trott, O.; Palmer, A. G. *J. Magn. Reson.* **2002**, *154*, 157−160.

used for the correction of resonance offset effects, spin-lock field inhomogeneity, and power losses after long rf irradiation.[23] Systematic biases may also be introduced into R_2 values measured in spin−echo experiments due to off-resonance effects of π pulses in CPMG pulse trains,[24,25] and a recent report[24] has described how such artifacts can be corrected, yielding accurate transverse relaxation rates. Increased R_2 rates obtained from $R_{1\rho}$ measurements relative to those measured from CPMG-based pulse sequences, R_2(CPMG), were noted in several backbone ^{15}N relaxation studies[24,26,27] and could not be explained by properly taking into account off-resonance effects in the CPMG experiments.[24]

Cross-correlation between dipole−dipole and chemical shift anisotropy (CSA) relaxation mechanisms complicates the measurement of heteronuclear autorelaxation rates in protein ^{15}N−^{1}H and ^{13}C−^{1}H spin pairs.[28−30] The application of either proton π pulses or proton composite pulse decoupling schemes (e.g., WALTZ16[31]) essentially eliminates these cross-correlation effects in heteronuclear R_2(CPMG) and $R_{1\rho}$ experiments,[29,30] although elevated R_2(CPMG) values resulting from imperfections in decoupling have been reported.[29,30] In the present contribution we show that the use of either ^{1}H π pulses or ^{1}H decoupling during the spin-lock period can lead to systematic overestimations of heteronuclear $R_{1\rho}$ values, potentially compromising their use in the characterization of protein dynamics. Herein, we describe the origin of such artifacts and illustrate both with experimental and simulated data that the effects can be substantial. Subsequently, simple experimental pulse schemes are presented which remove cross-correlation effects without introducing systematic bias in $R_{1\rho}$ values. These schemes are applied to the measurement of ^{15}N $R_{1\rho}$ values in protein L, a small folded domain composed of 63 residues.[32,33] Excellent correlations between R_2 rates measured via the CPMG experiment and the new $R_{1\rho}$ schemes are demonstrated.

Materials and Methods

Relaxation Measurements. ^{15}N Spin-relaxation measurements were performed on a sample of the spectrin SH3 domain[34] (6 mM in protein, pH 3.5, 90% H_2O, 10% D_2O, 1 μM leupeptin, 1 μM pepstatin, 800 μM Pefabloc, 278 K) at 11.7 T and on a sample of protein L (1.8 mM in protein, 50 mM sodium phosphate buffer, pH 6.0, 298 K) at 14.1 T. ^{15}N R_1 and R_2(CPMG) values were measured as described previously.[35]

^{15}N R_1 and R_2(CPMG) values of backbone amides in protein L were obtained by fitting the intensities of cross-peaks in a set of two-dimensional spectra recorded with different relaxation delays. Maximal delays employed were 750 and 200 ms for R_1 and R_2(CPMG), respectively, with the spacing between ^{15}N π pulses in the CPMG sequence set to 0.66 ms. The R_2(CPMG) values were numerically corrected to account for off-resonance effects associated with the CPMG refocusing pulses (B_1 field strength of 5.4 kHz), as described by Korzhnev et al.[24]

^{15}N $R_{1\rho}$ rates were obtained using the pulse sequence shown in Figure 1. The essential elements of the pulse scheme have been described previously[18] and will not be repeated here. Note that during the spin-lock period of duration T magnetization from each ^{15}N spin is placed along an effective field given by the vector sum of the rf (B_1) field and the residual Zeeman field, which differs for each distinct ^{15}N nucleus. This is achieved in all experiments described in the present work using scheme 1 of Figure 1 in which chemical shift precession occurs for fixed delays, described in detail elsewhere.[18,36,37] Placement of the magnetization in this direction ensures that there is little sensitivity loss due to rf field inhomogeneity which would lead to the rapid decay of the component of the signal that is orthogonal to the effective spin-lock axis. An improved version of the experiment, described in Mulder et al.[20] (scheme 2 in Figure 1), uses adiabatic pulses to achieve alignment of magnetization vectors from individual amide sites along their effective fields. The conclusions obtained in the present study with regard to the experimental schemes of Figure 1 are equally valid for sequences which use these adiabatic pulses.

To assess the efficacy of a number of different approaches for suppression of cross-correlation between ^{15}N−^{1}H dipolar and ^{15}N CSA relaxation mechanisms we have used the sequence of Figure 1, with various suppression methods represented by inserts a−d. The HN$^{\epsilon}$ proton of Trp41 in the spectrin SH3 domain is well resolved, and the $R_{1\rho}$ relaxation rate of the side chain ^{15}N indole spin of this residue can therefore be obtained rapidly by recording a series of one-dimensional spectra with variable spin-lock times, T (Figure 1). ^{15}N$^{\epsilon}$ $R_{1\rho}$ values were obtained by exponential fitting of signal decays composed of at least 12 data points (T values ranging from 10 to 180 ms). In addition we have also measured ^{15}N$^{\epsilon}$ R_1 and R_2(CPMG) rates for this residue with the ^{15}N carrier placed on resonance. $R_{1\rho}$ values for all of the backbone ^{15}N spins of protein L were obtained from a set of two-dimensional $R_{1\rho}$ spectra with a maximum spin-lock duration of 120 ms. In all cases ^{15}N R_2 values were obtained from measured $R_{1\rho}$ and R_1 rates according to $R_2 = (R_{1\rho} - R_1 \cos^2 \theta_S)/\sin^2 \theta_S$, where $\theta_S = \text{arccot}(\Omega_S/\nu_{1S})$, ν_{1S} is ^{15}N spin-lock field strength (in Hz), and Ω_S is the resonance offset from the spin-lock carrier (Hz).

We have also extended our studies to include measurements of ^{13}C R_1, R_2(CPMG), and $R_{1\rho}$ rates in ^{13}C−^{1}H spin pairs. Specifically in this case, all experiments were performed on a sample of fractionally deuterated pyruvate labeled with ^{13}C at the methyl position, dissolved in deuterated glycerol. Pulse schemes, analogous to the sequence described by Ishima et al.[38] have been employed, with selection of methyl isotopomers of the form $^{13}CHD_2$, so that ^{13}C relaxation in an AX spin system (to good approximation) could be investigated. All experiments on pyruvate were recorded at 278 K at 11.7 T with spin-lock periods T varying from 0 to 128 ms.

The spin-lock field strengths used in the $R_{1\rho}$ experiments were calibrated according to the method of Desvaux and co-workers.[23] On the probes used in this study the resulting ν_{1S} distributions are almost symmetric with center (Hz)/half-width (Hz) of 1170/45 (^{15}N, spectrin SH3 domain, 11.7 T), 1630/65 (^{15}N, protein L, 14.1 T) and 1810/60 (^{13}C, pyruvate, 11.7 T).

Numerical Simulations. Simulations of spin dynamics in the $R_{1\rho}$ experiments of Figure 1 were performed by numerical solution of the

(23) Guenneugues, M.; Berthault, P.; Desvaux, H. *J. Magn. Reson.* **1999**, *136*, 118−126.
(24) Korzhnev, D. M.; Tischenko, E. V.; Arseniev, A. S. *J. Biomol. NMR* **2000**, *17*, 231−237.
(25) Ross, A.; Czisch, M.; King, G. C. *J. Magn. Reson.* **1997**, *124*, 355−365.
(26) Lee, B. M.; De Guzman, R. N.; Turner, B. G.; Tjandra, N.; Summers, M. F. *J. Mol. Biol.* **1998**, *279*, 633−649.
(27) Lee, A. L.; Wand, A. J. *J. Biomol. NMR* **1999**, *13*, 101−112.
(28) Boyd, J.; Hommel, U.; Campbell, I. D. *Chem. Phys. Lett.* **1990**, *175*, 477−482.
(29) Palmer, A. G.; Skelton, N. J.; Chazin, W. J.; Wright, P. E.; Rance, M. *Mol. Phys.* **1992**, *75*, 699−711.
(30) Kay, L. E.; Nicholson, L. K.; Delaglio, F.; Bax, A.; Torchia, D. A. *J. Magn. Reson.* **1992**, *97*, 359−375.
(31) Shaka, A. J.; Keeler, J.; Frenkiel, T.; Freeman, R. *J. Magn. Reson.* **1983**, *52*, 335−338.
(32) Wikstrom, M.; Drakenberg, T.; Forsen, S.; Sjobring, U.; Bjorck, L. *Biochemistry* **1994**, *33*, 14011−14017.
(33) Scalley, M. L.; Yi, Q.; Gu, H. D.; McCormack, A.; Yates, J. R.; Baker, D. *Biochemistry* **1997**, *36*, 3373−3382.
(34) Blanco, F. J.; Ortiz, A. R.; Serrano, L. *J. Biomol. NMR* **1997**, *9*, 347−357.
(35) Farrow, N. A.; Muhandiram, R.; Singer, A. U.; Pascal, S. M.; Kay, C. M.; Gish, G.; Shoelson, S. E.; Pawson, T.; Formankay, J. D.; Kay, L. E. *Biochemistry* **1994**, *33*, 5984−6003.
(36) Griesinger, C.; Ernst, R. R. *J. Magn. Reson.* **1987**, *75*, 261−271.
(37) Yamazaki, T.; Muhandiram, R.; Kay, L. E. *J. Am. Chem. Soc.* **1994**, *116*, 8266−8278.
(38) Ishima, R.; Louis, J. M.; Torchia, D. A. *J. Am. Chem. Soc.* **1999**, *121*, 11589−11590.

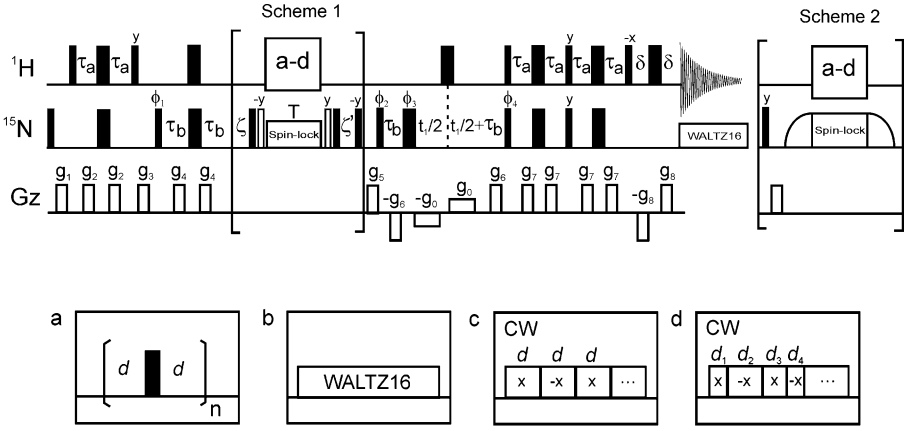

Figure 1. Pulse schemes for the measurement of ^{15}N $R_{1\rho}$ values. Scheme 1 is an experiment proposed by Akke and Palmer[18] while scheme 2 shows the improved sequence of Mulder et al.[20] Narrow (wide) solid bars correspond to $\pi/2$ (π) rf pulses applied with phase x, unless indicated otherwise, at a carrier frequency of ω_C. In scheme 1 the narrow open bars are ^{15}N pulses with flip angles of $\pi/2 - \arccot(\Omega/\nu_{1S})$, where ν_{1S} is the ^{15}N spin-lock field strength and Ω is the spin-lock offset from ω_C. The phases of these pulses are inverted when the sign of Ω changes. Note that the carrier is switched from ω_C to $\omega_C+\Omega$ immediately prior to T and then back right after. In scheme 2 adiabatic pulses are used to transfer magnetization from the z-axis to the off-resonance spin-lock field and vice versa, as described by Mulder et al. [20] (see this paper for details). Experiments in the present paper were recorded with scheme 1. All ^{1}H pulses, except those used to attenuate cross-correlation during the ^{15}N spin-lock, are applied with the carrier frequency centered on the water resonance. The CW and WALTZ16 [31] ^{1}H decoupling schemes (~5 kHz fields) are centered in the middle of the amide region. During the spin-lock interval of duration T an ^{15}N field of ~1.7 kHz is typically employed. A 1 kHz ^{15}N WALTZ16 decoupling field [31] is employed during acquisition. Values of the delays are $\tau_a = 2.25$ ms, $\tau_b = 1/(4J_{NH}) \approx 2.75$ ms, $\delta = 0.75$ ms, $2\pi\zeta = \nu_{1S}/(\Omega^2+\nu_{1S}^2)$, $2\pi\zeta' = \nu_{1S}/(\Omega^2+\nu_{1S}^2) - 2/\nu_N$, where ν_N is the field of the ^{15}N pulses. Gradient strengths in G/cm (length in ms) are $g_0 = 0.4$ ($t_1/2$), $g_1 = 5.0$ (1.0), $g_2 = 4.0$ (0.5), $g_3 = 10.0$ (1.0), $g_4 = 8.0$ (1.0), $g_5 = 25.0$ (1.0), $g_6 = 15.0$ (1.25), $g_7 = 4.0$ (0.5), $g_8 = 14.8$ (0.125). The phase cycle employed is $\phi_1 = (x,-x)$, $\phi_2 = (y)$, $\phi_3 = 2(x)$, $2(y)$, $2(-x)$, $2(-y)$, $\phi_4 = (x)$, $\phi_{rec} = (x,-x,-x,x)$, with the spin-lock field applied along the x-axis. For each t_1 increment axial peaks are shifted to the border of the spectrum by inversion of ϕ_2 in concert with the receiver phase ϕ_{rec}.[52] Quadrature detection in F_1 is achieved using the enhanced sensitivity approach,[53,54] whereby separate spectra are recorded with (ϕ_4,g_6) and ($\phi_4+\pi$,$-g_6$) for each t_1 value. The ^{15}N spin-lock is applied during the period T with ^{15}N magnetization aligned along the effective field in the rotating frame as discussed by Griesinger and Ernst,[36] Yamazaki et al.[37] and Akke and Palmer.[18] The different ^{1}H sequences that have been used to suppress cross-correlation during the ^{15}N spin-lock interval, T, are illustrated in panels a−d. ^{1}H π pulses separated by delays $2d$ are applied in scheme a, scheme b uses ^{1}H WALTZ16 decoupling, while sequences c and d employ ^{1}H continuous wave (CW) irradiation. In scheme c the phase of the ^{1}H CW field is alternated between x and $-x$ every d ms (typically $d = 10$ ms), while in sequence d alternation is random, with d_i typically 10 ms, on average. Details of the implementation of the random phase alternation procedure are available upon request. Briefly, the pulse sequence code allows the user to define a basic interval of duration τ during which the phase of the CW field is fixed. Thus, if $T = \tau$ a CW field of phase x is applied, while if $T = 2\tau$, then a single phase change (from x to $-x$) occurs at some random time. If $T = k\tau$, there are $(k - 1)$ changes in phase during the spin-lock interval, so that $d_i \approx \tau$ on average. The code developed can be easily ported from Varian spectrometers as long as it is possible to access a random number generator from calls inside the pulse sequence.

Liouville−von Neumann equation.[39] We have considered an isolated two-spin system consisting of a proton I and heteronucleus S (^{15}N or ^{13}C) relaxed by dipole−dipole and CSA (S only) mechanisms. Cross-correlation between the $I-S$ dipolar, S CSA interactions has been taken into account, with the explicit expression for the elements of the Redfield relaxation matrix described elsewhere.[1] During the course of a pulse sequence the spin density operator, $\rho(t)$, evolves under the effect of Hamiltonians accounting for (i) chemical shift evolution, $H_{CS} = 2\pi\Omega_I I_Z + 2\pi\Omega_S S_Z$, where Ω_I and Ω_S are resonance offsets for spins I and S, (ii) scalar coupling, $H_J = 2\pi J I_Z S_Z$, where J is the scalar coupling constant in Hz, and (iii) rf fields, $H_{rf} = 2\pi\nu_{1I} I_X + 2\pi\nu_{1S} S_X$, where ν_{1I} and ν_{1S} are the strengths of rf fields applied at or near the frequencies of spins I and S, respectively. The density operator at the beginning of spin lock, $\rho(0)$, is given by $S_Z' = S_X \sin\theta_S + S_Z \cos\theta_S$ where $\theta_S = \arccot(\Omega_S/\nu_{1S})$, corresponding to magnetization of heteronucleus S locked along its effective field in the rotating frame.

Numerical simulations have been performed for ^{15}N−^{1}H and ^{13}C−^{1}H groups using values of −90 Hz for NH and 140 Hz for CH J-coupling constants. In some cases (see Figure 2) simulations were compared directly to experiment, and parameters used were identical to those employed in experiment. In addition, dynamics parameters used in the computations were adjusted so as to reproduce the measured R_1 and R_2(CPMG) relaxation rates. Simulations of the experimental $R_{1\rho}$ profiles for the N$^\epsilon$ spin of Trp41 of the spectrin SH3 domain (Figure 2) were based on auto- and cross-relaxation rates calculated using an overall tumbling time, $\tau_R = 10.1$ ns and an order parameter, $S^2 = 0.93$ along with $r_{NH} = 1.02$ Å and ^{15}N$^\epsilon$ CSA parameters of $\sigma_{11} = -62.8$ ppm, $\sigma_{22} = 5.8$ ppm and $\sigma_{33} = 57.0$ ppm,[40] where σ_{ii} is the ith principal component of the ^{15}N CSA tensor and σ_{33} is directed along the NH bond. All calculations made use of the simplest form of the Lipari−Szabo spectral density function,[41] with the correlation time for fast local motion set to 0.

Additional simulations for ^{15}N−^{1}H groups (Figures 3, 4, and 6) have also been carried out using either 1.0 or 2.0 kHz ^{15}N spin-lock fields, that are either homogeneous or inhomogeneous with a distribution of field strengths given by the relation $\exp(-(x - x_o)^2/s^2)$, where $x_o = 1$ or 2 kHz, $s = 50$ Hz. Note that rf inhomogeniety of ^{1}H pulses and ^{1}H CW decoupling fields have not been taken into account in any of the simulations. Backbone ^{15}N relaxation rates were generated assuming $\tau_R = 5.0$ ns and an axially symmetric CSA tensor with $\Delta\sigma = -160$ ppm.[42] All of these simulations used a 35.7 kHz rf field for ^{1}H pulses or a 5.0 kHz ^{1}H decoupling field.

In the case of simulations involving the relaxation of the ^{13}C methyl carbon in $^{13}CHD_2$ isotopomers in pyruvate, values of $\tau_R = 5.0$ ns, $S^2 = 0.17$, $r_{CH} = 1.09$ Å and an axially symmetric ^{13}C CSA tensor with $\Delta\sigma = 25$ ppm [14] were found to exactly reproduce experimental ^{13}C R_1 and R_2(CPMG) rates. Note that three-fold rotation about the methyl-averaging-axis sets an upper bound for S^2 of 0.111, indicating that methyl rotation may be hindered in pyruvate or, alternatively, that the Lipari−Szabo model used to interpret the dynamics may well be overly simplistic, requiring more complex spectral density functions (along

(39) Ernst, R. R.; Bodenhausen, G.; Wokaun, A. *Principles of Nuclear Magnetic Resonance in One and Two Dimensions*; Oxford University Press: Oxford, 1987.

(40) Ramamoorthy, A.; Wu, C. H.; Opella, S. J. *J. Am. Chem. Soc.* **1997**, *119*, 10479−10486.
(41) Lipari, G.; Szabo, A. *J. Am. Chem. Soc.* **1982**, *104*, 4546−4559.
(42) Hiyama, Y.; Niu, C. H.; Silverton, J. V.; Bavoso, A.; Torchia, D. A. *J. Am. Chem. Soc.* **1988**, *110*, 2378−2383.

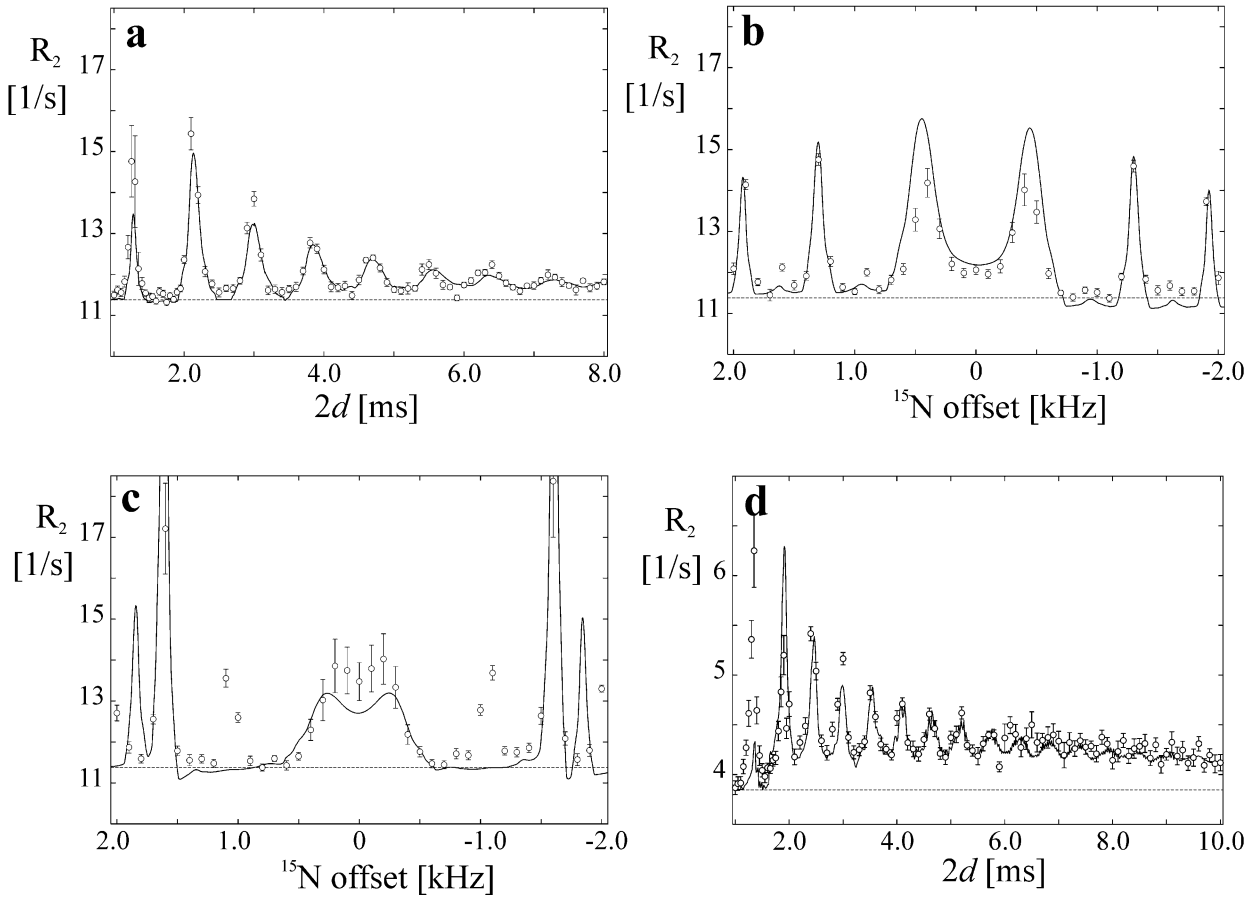

Figure 2. Experimental (open circles) and simulated (solid lines) transverse relaxation rates, R_2, obtained from $R_{1\rho}$ values of (i) the $^{15}N^{\epsilon}$ spin of Trp41 in the spectrin SH3 domain (a−c) and of (ii) the ^{13}C spin of the $^{13}CHD_2$ group of pyruvate (d). Dashed lines in the plots denote the R_2 value measured using a CPMG-based pulse scheme with $^{15}N/^{13}C$ π pulses applied on-resonance. Dipole−dipole/CSA cross-correlation in the $R_{1\rho}$ experiments is suppressed by ^1H π pulses [29,30] (plots a,b,d) or by ^1H WALTZ16 decoupling [29] (plot c) applied during the $^{15}N/^{13}C$ spin-lock interval. (a) $^{15}N^{\epsilon}$ R_2 vs ^1H inter-pulse delay, $2d$, measured using an on-resonance 1.17 kHz ^{15}N spin-lock; (b) $^{15}N^{\epsilon}$ R_2 vs ^{15}N offset from the spin-lock carrier for $2d = 2$ ms and a field of 1.17 kHz. (c) ^{15}N R_2 vs ^{15}N offset using a 4.6 kHz ^1H WALTZ16 decoupling field to suppress cross-correlation and a 1.17 kHz spin-lock field; (d) ^{13}C R_2 versus $2d$ measured with a 1.8 kHz on-resonance ^{13}C spin-lock. ^{15}N and ^{13}C $R_{1\rho}$ values were simulated as described in Materials and Methods using distributions of the spin-lock fields (i.e., rf inhomogeneity) measured according to Desvaux and co-workers.[23]

with additional relaxation measurements) for the interpretation of the measured rates. However, since the goal of the present work is not to obtain insight into the dynamics of pyruvate in solution but rather to be able to simulate the artifacts observed experimentally in $R_{1\rho}$ measurements, we were satisfied with the above set of dynamics parameters.

In all simulations the apparent $R_{1\rho}$ relaxation rate was obtained from the decay of the magnetization along the effective spin-lock field. Twenty values of the magnetization at time points ranging from $T = 0$ to 200 ms were obtained by projecting the density operator onto $S_x \sin\theta_S + S_z \cos\theta_S$, and these values subsequently fitted with a single-exponential decay function, $A \exp(-R_{1\rho}T)$.

Results and Discussion

Standard Methods for Suppression of Cross-Correlation Result in Overestimated $R_{1\rho}$. It has long been recognized that cross-correlation between X−H dipolar and X chemical shift anisotropy relaxation interactions can have a significant impact on measured heteroatom spin-relaxation rates.[28−30] For example, for an $^{15}N-^1H$ spin pair attached to a protein tumbling isotropically in solution with a correlation time of 9 ns it was shown that cross-correlation can lead to an underestimation of the transverse autorelaxation decay rate of the ^{15}N spin by approximately 25% for measurements recorded at 11.7 T.[30] The effects of dipole−CSA cross-correlation can be eliminated in transverse spin-relaxation experiments by the application of ^1H π pulses at a rate that prevents the flow of in-phase to anti-phase magnetization (from S_X to $2S_XI_Z$, for example)[29,30] or the application of decoupling fields.[29] Both methods are used in measurements of $R_{1\rho}$ relaxation rates (Figure 1a,b), and as we show below through results obtained from both simulation and experiment substantial systematic errors can result.

Figure 2a−c shows experimental (circles) R_2 values calculated from measured $R_{1\rho}$ rates (see Materials and Methods) for the $^{15}N^{\epsilon}$ of Trp41 in the spectrin SH3 domain along with the corresponding values obtained from simulation (solid lines). In Figure 2a the scheme of Figure 1a has been employed with an ^{15}N *on-resonance* spin-lock field of 1.17 kHz and a spacing between successive ^1H π pulses given by $2d$ (horizontal axis). The dashed line in Figure 1 indicates the R_2(CPMG) value obtained with on-resonance heteroatom π pulses applied during the CPMG pulse train. In what follows, the R_2(CPMG) values are assumed to be error-free, justified by the conclusions of this work. Good agreement is noted between experimental and simulated R_2 values obtained from $R_{1\rho}$ rates, with large discrepancies observed between R_2 rates obtained from $R_{1\rho}$ and CPMG-based approaches. At first glance the dependence of R_2 values generated from spin-lock methods on the rate of application of ^1H pulses seems counterintuitive since the

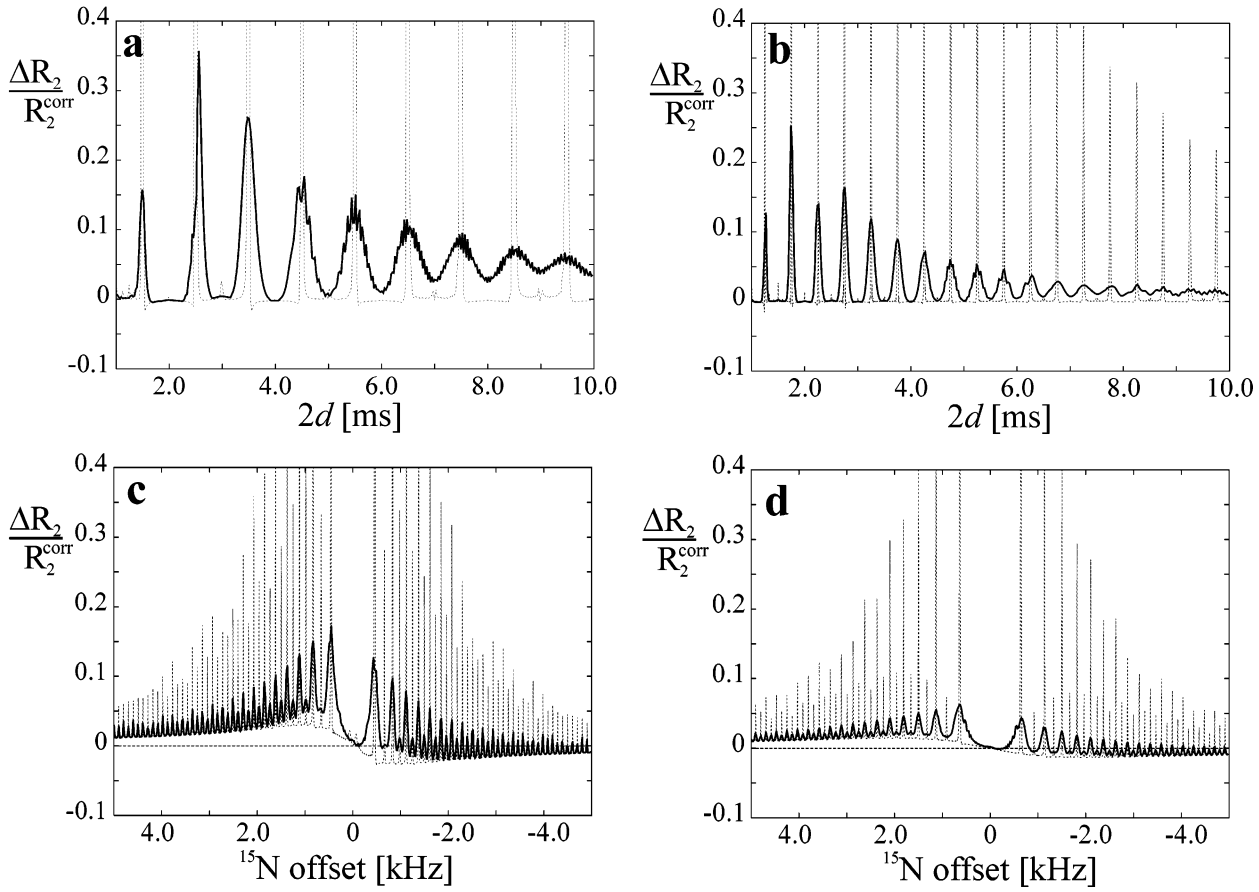

Figure 3. Systematic errors in ^{15}N R_2 values obtained from $R_{1\rho}$ measurements when regularly spaced ^{1}H π pulses are applied during the ^{15}N spin-lock. In the ratio $\Delta R_2/R_2^{corr}$, $\Delta R_2 = R_2^{calc} - R_2^{corr}$, R_2^{corr} is the actual transverse relaxation rate, R_2^{calc} is the apparent transverse relaxation rate obtained from the simulated $R_{1\rho}$ data, as described in the text. In the simulations a 1.0 kHz (plots a,c) or 2.0 kHz (plots b,d) spin-lock field is employed, which is either assumed to be homogeneous (dashed lines) or inhomogeneous with a distribution given by the relation $\exp(-(x - x_o)^2/s^2)$, where x_o is the B_1 spin-lock field strength and $s = 50$ Hz (bold solid lines). (a), (b) $\Delta R_2/R_2^{corr}$ vs ^{1}H inter-pulse spacing, $2d$, using an on-resonance ^{15}N spin-lock; (c), (d) $\Delta R_2/R_2^{corr}$ vs ^{15}N offset from the spin-lock carrier with $2d = 5$ ms.

magnetization of interest during the spin-lock period is pure in-phase, S_X, but as we show below these effects can be easily explained.

Figure 2b illustrates the R_2 profile obtained as a function of offset with an ^{15}N spin-lock field, ν_{1S}, of 1.17 kHz, $2d = 2$ ms. In this figure a positive offset corresponds to the carrier positioned upfield of the Trp 41 $^{15}N^{\epsilon}$ resonance. In Figure 2c the pulse scheme of Figure 1b has been employed with a ^{1}H WALTZ16 decoupling field of 4.6 kHz. As in the case of suppression of cross-correlation through the application of ^{1}H π pulses (Figure 1a) large errors result when continuous decoupling fields are applied as well.

The errors in $R_{1\rho}$ are not limited to measurements of ^{15}N spin relaxation. Figure 2d shows experimental and simulated data from the $^{13}CHD_2$ methyl of a fractionally deuterated pyruvate sample obtained with a 1.8 kHz on-resonance spin-locking field with ^{1}H π pulses applied every $2d$ ms, and it is clear that substantial errors in ^{13}C R_2 rates occur as well.

To investigate how errors in R_2 values depend on parameters such as rf inhomogeneity and spin-locking field strength we have carried out a number of additional numerical simulations for isolated ^{15}N−^{1}H spin pairs. In all of the simulations we have assumed a ^{15}N spin attached to a molecule tumbling isotropically with a correlation time of 5 ns. Figure 3a−d shows $(\Delta R_2)/(R_2^{corr})$, where ΔR_2 is the difference between an R_2 value calculated from a simulated $R_{1\rho}$ rate and the correct value used in simulations, R_2^{corr}, for spin-lock fields of 1 and 2 kHz. The bold lines correspond to simulations carried out including the effects of inhomogeneity, modeled as described in Materials and Methods, while the dashed lines assume perfectly homogeneous fields. Errors decrease as a function of increasing spin-lock field and can be completely eliminated in simulations by setting the value of the heteronuclear scalar coupling constant, J, to zero. When inhomogeneity is taken into account, the magnitude of the errors decreases although the range of delays $2d$ and ^{15}N offsets over which errors are observed becomes significantly larger. Of interest, application of ^{1}H π pulses leads to an asymmetry in the offset dependence of $R_{1\rho}$ (Figure 3c), $\nu_{1S} = 1$ kHz, $2d = 5$ ms and (Figure 3d) $\nu_{1S} = 2$ kHz, $2d = 5$ ms. This asymmetry can be eliminated by setting J to zero or by neglecting ^{15}N−^{1}H dipolar, ^{15}N CSA relaxation interference, although the precise origin of this effect remains to be investigated.

Figure 4a−c shows simulations of the time evolution of ^{15}N magnetization in an isolated ^{15}N−^{1}H spin system during an on-resonance homogeneous spin-lock of 1 kHz for $2d$ values of 1.5 (solid line) and 3.5 ms (dashed line). In the case where ^{1}H π pulses are not applied and cross-correlation between dipole and CSA interactions are neglected, single exponential decays of S_X are observed, while the terms $2S_YI_Z$ and $2S_ZI_Z$ are not

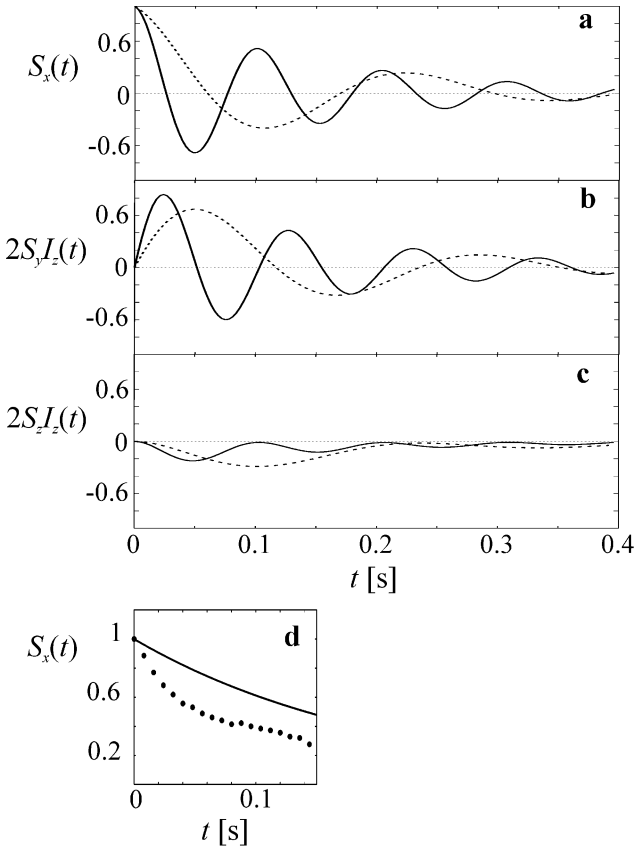

Figure 4. Simulation of the evolution of (a) S_X, (b) $2S_YI_Z$, and (c) $2S_ZI_Z$ operators (I − ^{1}H, S − ^{15}N) during application of a 1 kHz on-resonance homogeneous spin-lock field with ^{1}H π pulses applied every 1.5 ms (solid line) or 3.5 ms (dashed line). The simulations consider all 16 basis operators necessary to describe the complete evolution of an isolated two-spin system (see Materials and Methods). At $t = 0$ magnetization is of the form S_X, and the length of the magnetization vector is set to 1. Note that a "local field" treatment (see text) predicts identical time behavior for S_X. In the case when ^{1}H π pulses are not applied or in the absence of cross-correlation, an exponential decay of S_X is obtained with a rate of 8.1 s^{-1}. (d) Experimental time dependence of the evolution of S_X obtained for the ^{15}N$^\epsilon$ spin of Trp41 of the spectrin SH3 domain during application of an on-resonance 1.17 kHz spin-lock field and ^{1}H π pulses every 1.5 ms (solid circles) and the exponential decay expected based on R_2(CPMG) data (solid line).

produced at all (not shown). In contrast, when ^{1}H π pulses are applied, the decay of S_X is strongly modulated which results in an apparent increase in measured $R_{1\rho}$ values if the signal (over intervals from 0 to 200 ms, for example) is fitted to an exponential decay function (see below). Of note, the transfer of magnetization from S_X to I_X is effectively blocked during the spin-lock period. Simulations show, for example that for $2d = 3.5$ ms and starting from $S_X = 1$ at $t = 0$, I_X or I_Y terms with magnitudes of no more than 3×10^{-5} are created. Thus, the oscillations in signal observed in Figure 4a,b do not derive from the Hartmann−Hahn effect where magnetization transfers effectively between scalar coupled spins[39] (i.e., from S to I, see below). Figure 4d shows the time dependence of S_X for the ^{15}N$^\epsilon$ spin of Trp41 of the spectrin SH3 domain measured using an on-resonance spin-lock field of 1.17 kHz with $2d = 1.5$ ms (circles) along with the exponential decay expected based on R_2(CPMG) measurements (solid line). The oscillations are much less pronounced in the experimental profile since the B_1 field is not perfectly homogeneous.

Errors in R_2 rates measured using spin-lock-based experiments are expected to have a significant effect on dynamics parameters extracted from R_1, R_2, and heteroatom NOE values. For example, overestimation of R_2 leads to excessively large values for the overall rotational correlation time τ_R extracted from R_2/R_1 ratios[43] and to erroneous values of order parameters and correlation times describing internal dynamics.[1,44,45] The artifactual offset-dependence of R_2 values noted in Figure 2b,c complicates the extraction of accurate microsecond-to-millisecond time scale dynamics parameters from off-resonance $R_{1\rho}$ experiments. With these problems in mind we turn our attention now to describing the origin of the errors using a simple "local field" model and subsequently present a pulse scheme to eliminate them.

Modeling the Effects of ^{1}H π Pulses Using a "Local-Field" Approximation. The numerical simulations shown in Figures 2−4 have been performed in a space of 16 product operators that describes the complete evolution of an isolated two spin−$^1/_2$ spin system. To obtain a physical picture of the effects of ^{1}H π pulses on the evolution of magnetization during a spin-lock period, however, it is more convenient to simplify the problem by using a "local-field" approach. In this formulation a single isolated spin S (heteronucleus) is considered in the presence of local fields resulting from the scalar coupled spin I (proton). These local fields can be included in a simple manner by additional Hamiltonians, H_{LF}, which have the same form as the S chemical shift Hamiltonian, $H_{LF} = \pi JS_Z$ and $H_{LF} = -\pi JS_Z$ corresponding to spin I in the $^1/_2$ (α) or $-^1/_2$ (β) state, respectively. Consider S magnetization at an offset of Ω_S Hz from the carrier so that the effective residual Zeeman field for each of the S doublet components is given by $\Omega_S+J/2$ (I spin in the α state) and $\Omega_S-J/2$ (I spin in the β state). In what follows we refer to S spin magnetization coupled to α and β ^{1}H spin states at the start of the spin-lock period by $S_{1/2}$ and $S_{-1/2}$, respectively. Immediately prior to the spin-lock period of duration T in Figure 1 S spin magnetization is aligned along the effective field, $\mathbf{n} = (\nu_{1S},0,\Omega_S)/\nu$, where ν_{1S} is the magnitude (Hz) of the spin-lock field applied along the x-axis and ν is the effective frequency, $\nu = \sqrt{\nu_{1S}^2+\Omega_S^2}$. Note, however, that the artifacts described above would be present, irrespective of the initial placement of S magnetization.

The evolution of $S_{1/2}$ during the spin-lock period in which ^{1}H π pulses are applied along the x-axis according to the scheme $(d-\pi_x(I)-d-d-\pi_x(I)-d)_n$, Figure 1a, can be calculated as a series of $3n$ consecutive rotations of the magnetization $S_{1/2}$ according to the following: (i) rotate about the vector $\mathbf{n}_{1/2} = (\nu_{1S},0,\Omega_S + J/2)/\nu_{1/2}$ with a frequency $\nu_{1/2} = \sqrt{\nu_{1S}^2+(\Omega_S+J/2)^2}$ for a time d, (ii) subsequently rotate about $\mathbf{n}_{-1/2} = (\nu_{1S},0,\Omega_S-J/2)/\nu_{-1/2}$ with a frequency $\nu_{-1/2} = \sqrt{\nu_{1S}^2+(\Omega_S-J/2)^2}$ for a time $2d$ and (iii) rotate about $\mathbf{n}_{1/2}$ with a frequency $\nu_{1/2}$ for an additional period of time d, (iv) repeat steps (i−iii) n times. Note that the effect of ^{1}H π pulses during the spin-lock interval is to invert the sign of the local-field Hamiltonian so that rotation axes and frequencies alternate between $\mathbf{n}_{1/2},\nu_{1/2}$ and $\mathbf{n}_{-1/2},\nu_{-1/2}$, respectively. A similar set of rotations can be performed for $S_{-1/2}$, and the net magnetization at the end of the spin-lock interval is given by the sum of the two spin S components.

(43) Kay, L. E.; Torchia, D. A.; Bax, A. *Biochemistry* **1989**, *28*, 8972−8979.
(44) Korzhnev, D. M.; Orekhov, V. Y.; Arseniev, A. S. *J. Magn. Reson.* **1997**, *127*, 184−191.
(45) Orekhov, V. Y.; Pervushin, K. V.; Korzhnev, D. M.; Arseniev, A. S. *J. Biomol. NMR* **1995**, *6*, 113−122.

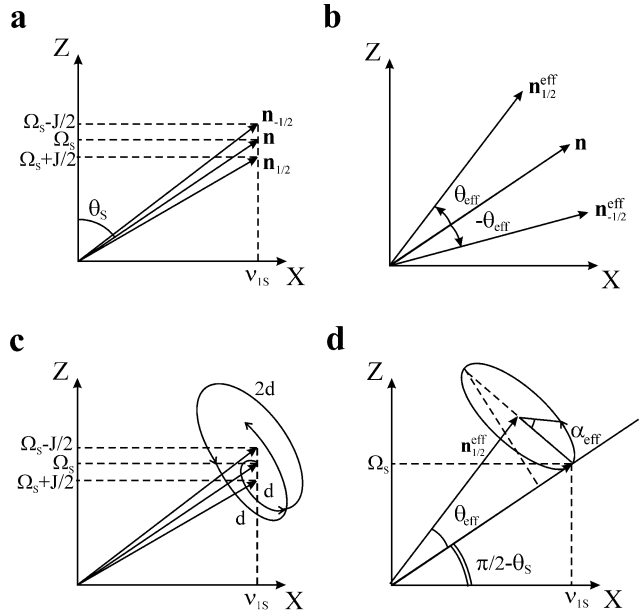

Figure 5. Schematic representation of effective fields described in the text (a, b) and the rotations of magnetization about these fields during the spin-locking interval in an $R_{1\rho}$ experiment. (a) Vectors $\mathbf{n} = (\nu_{1S},0,\Omega_S)/\nu$, $\mathbf{n}_{1/2} = (\nu_{1S},0,\Omega_S+J/2)/\nu_{1/2}$ and $\mathbf{n}_{-1/2} = (\nu_{1S},0,\Omega_S-J/2)/\nu_{-1/2}$, with $\nu = \sqrt{\nu_{1S}^2+\Omega_S^2}$, $\nu_{1/2} = \sqrt{\nu_{1S}^2+(\Omega_S+J/2)^2}$ and $\nu_{-1/2} = \sqrt{\nu_{1S}^2+(\Omega_S-J/2)^2}$. In the scheme of Figure 1 magnetization is placed along **n** at the start of the spin-lock period and subsequently evolves due to application of ^{1}H π pulses. (b) After each successive $(d-\pi_x(I)-d-d-\pi_x(I)-d)$ interval the evolution can be described in terms of rotations about axes $\mathbf{n}^{eff}_{1/2}$ and $\mathbf{n}^{eff}_{-1/2}$ for S magnetization coupled to proton spins in the α ($S_{1/2}$) and β ($S_{-1/2}$) states, respectively. (c) Actual trajectory of $S_{1/2}$ during a $(d-\pi_x(I)-d-d-\pi_x(I)-d)$ element, with magnetization originating along **n**. (d) Effective rotation about the axis $\mathbf{n}^{eff}_{1/2}$ by the angle α_{eff} corresponding to the sum of the three rotations shown in plot c. The angles θ_{eff} and α_{eff} are given in eq 3. The figure has been prepared assuming that J is negative.

Figure 5a illustrates the relative positions of vectors $\mathbf{n}_{1/2}$, $\mathbf{n}_{-1/2}$, and **n** in the $X-Z$ plane for the case of $J < 0$.

The sequence of rotations listed above, (i−iv), describing the evolution of $S_{1/2}$ can be expressed in terms of a series of unitary transformations where the magnetization vector $S_{1/2}(t)$, sampled stroboscopically, is given at the end of the period of time $4dn$, as

$$S_{1/2}(4dn) = (U)^n S_{1/2}(0)(U^{-1})^n \tag{1}$$

where $U = U_{(iii)}U_{(ii)}U_{(i)}$ and $U_{(i)}$, $U_{(ii)}$, $U_{(iii)}$ are rotations described in each of steps (i−iii) listed above. We can replace $(U)^n$ with a single effective rotation of α_{eff} about the axis $\mathbf{n}_{eff}$, and it can be shown that this effective axis lies in the XZ plane (see below). In a similar manner α_{eff} and $\mathbf{n}_{eff}$ can be obtained for $S_{-1/2}$.

To calculate $\mathbf{n}_{eff}$ and α_{eff} for $S_{1/2}$ and $S_{-1/2}$ we have used the formula for combining successive rotations of angles Φ_1 and Φ_2 about axes $\mathbf{n}_1$ and $\mathbf{n}_2$ into a single rotation of angle α_{rot} about an axis $\mathbf{n}_{rot}$,[46]

$$\mathbf{n}_{rot} = (s_1c_2\mathbf{n}_1 + c_1s_2\mathbf{n}_2 - s_1s_2\mathbf{n}_1\times\mathbf{n}_2)/s_{rot} \tag{2.1}$$

$$c_{rot} = c_1c_2 - s_1s_2\mathbf{n}_1\mathbf{n}_2 \tag{2.2}$$

In eq 2 c_i and s_i are equal to $\cos(\Phi_i/2)$ and $\sin(\Phi_i/2)$, respectively, $c_{rot} = \cos(\alpha_{rot}/2)$, $s_{rot} = \sin(\alpha_{rot}/2)$, and $\mathbf{n}_1$, $\mathbf{n}_2$, and $\mathbf{n}_{rot}$ are normalized. Successive application of eq 2 to consecutive rotations described in (i−iv) above gives for $\mathbf{S}_{1/2}$

$$\tan(\theta_{eff}) = -\left(\frac{J}{\nu}\right)\frac{\sin(\theta_S)\sin^2(\phi/2)}{\cos(\phi)} \tag{3.1}$$

$$\cos\left(\frac{\alpha_{eff}}{2n}\right) = \cos(2\phi) - \frac{1}{2}\left(\frac{J}{\nu}\right)^2 \sin^2(\theta_S)(\phi\cos(\phi) - \sin(\phi))\sin(\phi) \tag{3.2}$$

where only the leading terms in (J/ν), $\nu = \sqrt{\nu_{1S}^2+\Omega_S^2}$, have been retained. In eq 3 $\theta_S = \text{arccot}(\Omega_S/\nu_{1S})$, $\phi = 2\pi d\sqrt{\nu_{1S}^2+\Omega_S^2}$, α_{eff} is effective rotation angle, and θ_{eff} is the angle between the effective rotation axis $\mathbf{n}_{eff}$ in the XZ plane and **n**. Expressions for $S_{-1/2}$ can be obtained directly from eq 3 by replacing θ_{eff} with $-\theta_{eff}$. Figure 5b illustrates the spatial relationship between $\mathbf{n}^{eff}_{1/2}$, $\mathbf{n}^{eff}_{-1/2}$, and **n**, where $\mathbf{n}^{eff}_{1/2}$ and $\mathbf{n}^{eff}_{-1/2}$ are the effective rotation axes pertaining to the evolution of $S_{1/2}$ and $S_{-1/2}$, respectively.

In the case that the spin-lock field is applied on-resonance exact equations for θ_{eff} and α_{eff} can be derived in compact form. In this case

$$\tan(\theta_{eff}) = \mp\frac{\sin(2\varphi)\sin^2(\psi/2)}{\cos^2(\varphi)\cos(\psi) + \sin^2(\varphi)} \tag{4.1}$$

$$\cos\left(\frac{\alpha_{eff}}{2n}\right) = \cos^2(\varphi)\cos(2\psi) + \sin^2(\varphi) \tag{4.2}$$

where $\varphi = \arctan(J/(2\nu_{1S}))$, $\psi = 2\pi d\sqrt{\nu_{1S}^2+(J/2)^2}$ and the $-(+)$ sign in eq 4.1 is selected for $S_{1/2}(S_{-1/2})$. The leading terms in a power series expansion of eq 4 with respect to J/ν_{1S} are identical to those in eq 3 with $\Omega_S = 0$, as expected.

Equations 3−4 show that after any integral number of elements $(d-\pi_x(I)-d-d-\pi_x(I)-d)$ $S_{1/2}$ and $S_{-1/2}$ lie on surfaces of cones, with axes tilted by θ_{eff} ($S_{1/2}$) and $-\theta_{eff}$ ($S_{-1/2}$) from the effective magnetic field direction, **n**. While it is tempting, therefore, to think of the magnetization components as evolving in a cone, the actual trajectory is more complicated, as indicated in Figure 5c for the case of $S_{1/2}$. Here the magnetization first precesses about $\mathbf{n}_{1/2}$ for a time d at a frequency of $\nu_{1/2}$, followed by precession about $\mathbf{n}_{-1/2}$ for a time $2d$ at a frequency of $\nu_{-1/2}$, and so forth. Despite the complexity of the path, the magnetization always returns to the surface of the cone at time points that are integral multiples of $4d$. Figure 5d illustrates the effective cone of precession for the $S_{1/2}$ component reflecting the idea of stroboscopic sampling at time points $4dn$.

As discussed above, at time points $4dn$ during the spin-lock period one-half of the magnetization effectively resides on the surface of a cone with axis defined by $\mathbf{n}^{eff}_{1/2}$, while the other half is on the surface of a second cone defined by $\mathbf{n}^{eff}_{-1/2}$ (Figure 5b). To excellent approximation the sum of the S magnetization components lies along the effective field **n**. However, this sum oscillates as $S_{1/2}$ and $S_{-1/2}$ precess on their respective cones so that the amount of "spin-locked" magnetization is less than what is expected. This, in turn, leads to increased measured $R_{1\rho}$ rates. For certain unfortunate combinations of d, J, Ω_S, and ν_{1S}, each magnetization component ($S_{1/2}$ and $S_{-1/2}$) can be driven far from

(46) Elliott, J. P.; Dawber, P. G. *Symmetry in Physics*; Macmillan: London, 1979; Vol. 2.

the direction of the effective field such that the relaxation measurement becomes severely compromised.

The modulation of S spin magnetization is most pronounced when $\mathbf{n}_{\pm 1/2}^{\mathrm{eff}}$ deviate most significantly from $\mathbf{n}$ (i.e., when $\theta_{\mathrm{eff}} = 90°$). Starting from eq 3 and assuming that $J/\nu \ll 1$ we readily obtain the approximate condition for the maximum modulation effect where the $R_{1\rho}$ rates are most in error, which can be expressed equivalently as,

$$4d = (2k+1)/\sqrt{\nu_{1S}^2 + \Omega_S^2} \tag{5.1}$$

or

$$\Omega_S = \pm\sqrt{((2k+1)/4d)^2 - \nu_{1S}^2} \tag{5.2}$$

where k is an integer. The values of d and Ω_S predicted by eq 5 are in perfect agreement with values of d and Ω_S that produce the maximum enhancements (spikes) of $R_{1\rho}$ in experiments and simulations (Figures 2 and 3).

For the case where $\theta_{\mathrm{eff}} \approx 90°$ $\mathbf{n}_{\pm 1/2}^{\mathrm{eff}}$ are very nearly perpendicular to $\mathbf{n}$ and precession of the $S_{1/2}$ and $S_{-1/2}$ components about $\mathbf{n}_{1/2}^{\mathrm{eff}}$ and $\mathbf{n}_{-1/2}^{\mathrm{eff}}$, respectively, leads to a cosine modulation of the net magnetization with a frequency given by ν_{mod} where $2\pi\nu_{\mathrm{mod}} = \alpha_{\mathrm{eff}}/(4dn)$ and

$$\nu_{\mathrm{mod}} = \left(\frac{\sin\theta_S}{4\pi d}\right)\left(\frac{J}{\nu}\right) \tag{6}$$

where only the leading term in (J/ν) has been retained. Consider for example a ^{15}N $R_{1\rho}$ experiment ($J_{\mathrm{NH}} \approx -90$ Hz) with the ^{15}N spin-lock applied on-resonance with a field strength of 1 kHz and $2d = 2.5$ ms. The ^{15}N magnetization decay measured in this experiment is, to good approximation described by $\exp(-R_{1\rho}t)\cos(2\pi\nu_{\mathrm{mod}}t)$, with $\nu_{\mathrm{mod}} = 5.7$ s^{-1}, similar to $R_{1\rho}$ rates measured in small proteins. Clearly, fitting this decay profile with a monoexponential function leads to a dramatic overestimation of the relaxation rate. Equation 6 predicts that the extent to which $R_{1\rho}$ is overestimated will decrease with increasing delays between ^{1}H π pulses ($2d$), higher spin-lock fields, ν_{1S}, and increasing offsets, Ω_S, in agreement with experiment and numerical simulations (Figures 2, 3). Examples of S spin signal modulations that can be expected from 1 kHz, homogeneous field, on-resonance spin-lock experiments have been given in Figure 4a−c obtained from simulations using the complete two-spin system basis set. An experimental profile of S signal decay is also shown (Figure 4d). It is noteworthy that the "local field" approximation considered here predicts the correct time dependence of S_X.

Improved Methods for the Suppression of Cross-Correlation in the Heteronuclear $R_{1\rho}$ Experiment. The simulations and experimental results described above establish the problems associated with measuring heteroatom $R_{1\rho}$ rates that are free of cross-correlation effects between dipolar and CSA interactions. Clearly, experimental approaches involving the use of ^{1}H π pulses applied at regular short-spaced intervals or ^{1}H WALTZ16 decoupling during the spin-lock interval are not good solutions. Although we have not examined other composite decoupling schemes here, it is expected that these will also prove problematic. We have therefore looked for alternative schemes which do not introduce systematic errors in measured $R_{1\rho}$ values

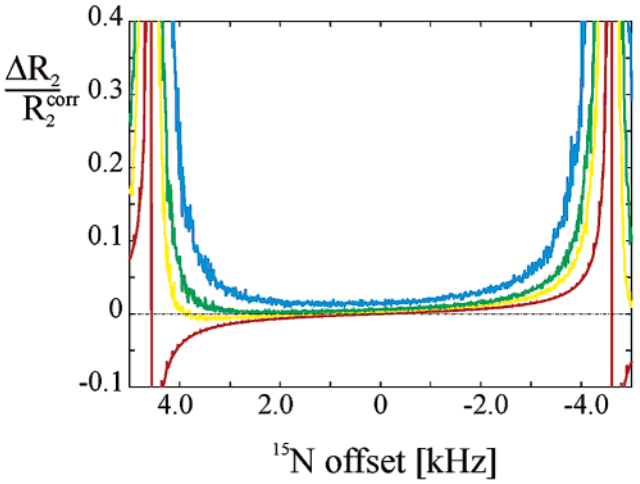

Figure 6. Simulated systematic errors in ^{15}N R_2 values obtained from $R_{1\rho}$ measurements when on-resonance ^{1}H CW fields are applied during the ^{15}N spin-lock interval. In the ratio $\Delta R_2/R_2^{\mathrm{corr}}$, $\Delta R_2 = R_2^{\mathrm{calc}} - R_2^{\mathrm{corr}}$, R_2^{corr} is the actual transverse relaxation rate, and R_2^{calc} is the apparent transverse rate obtained from the simulations. The ^{15}N $R_{1\rho}$ experiment is "simulated" as described in the Materials and Methods using a 2.0 kHz homogeneous spin-lock field. Values of $\Delta R_2/R_2^{\mathrm{corr}}$ are plotted as a function of ^{15}N offset from the spin-lock carrier using a 5.0 kHz ^{1}H CW field applied with phase x (red) and with phase alternated between x and $-x$ randomly, on average once per 10.0 ms (yellow), 5.0 ms (green), and 2.0 ms (blue).

while achieving good suppression of cross-correlation over the wide range of ^{15}N/^{13}C and ^{1}H chemical shift offsets that might be encountered in protein studies. Specifically we have examined a number of simple phase-modulated continuous wave (CW) ^{1}H irradiation schemes that might meet the requirements outlined above.

The simplest method to suppress cross-correlation is to apply a constant-phase CW ^{1}H field during the heteroatom spin-lock period. It is well-known that *on-resonance* ^{1}H CW irradiation completely suppresses ^{15}N−^{1}H dipolar/^{15}N CSA cross-correlation.[15] Both simulated (Figure 6, red) and experimental data (Figure 7a) establish that error-free $R_{1\rho}$ rates can be measured over a wide range of ^{15}N offsets as long as the Hartmann−Hahn coherence transfer condition,[47] $\Omega_I^2 + \nu_{1I}^2 = \Omega_S^2 + \nu_{1S}^2$, where ν_{1I} and ν_{1S} are ^{1}H and ^{15}N rf field strengths, respectively, is avoided. At typical ^{15}N spin-lock field strengths of 1−2 kHz and using 5−6 kHz on-resonance ^{1}H rf fields the matching condition given above is met for ^{15}N shifts of 4.5−6.0 kHz from the spin-lock carrier (see Figure 6), allowing precise $R_{1\rho}$ measurements for smaller offsets. Unfortunately, ^{1}H CW irradiation only attenuates X−H dipolar, X CSA cross-correlated cross-relaxation by the factor $\cos\theta_I$, where $\theta_I = \mathrm{arccot}(\Omega_I/\nu_{1I})$.[15] This level of suppression may be sufficient for accurate measurements of $R_{1\rho}$ values of ^{13}C$^\alpha$ or methyl ^{13}C spins in CHD_2 groups [38] due to their relatively small CSA values [1,14] and the small shift dispersion of the directly attached protons. However, for ^{15}N−^{1}H spin pairs in proteins suppression of cross-correlation by off-resonance ^{1}H rf fields is not satisfactory (see Figure 7b).

Figure 1c,d illustrates improved schemes for suppression of cross-correlation. In Figure 1c the phase of the ^{1}H CW irradiation field is inverted every d ms, while in Figure 1d the spin-lock period is divided into a series of intervals of random

(47) Hartmann, S. R.; Hahn, E. L. *Phys. Rev.* **1962**, *128*, 2042−2053.

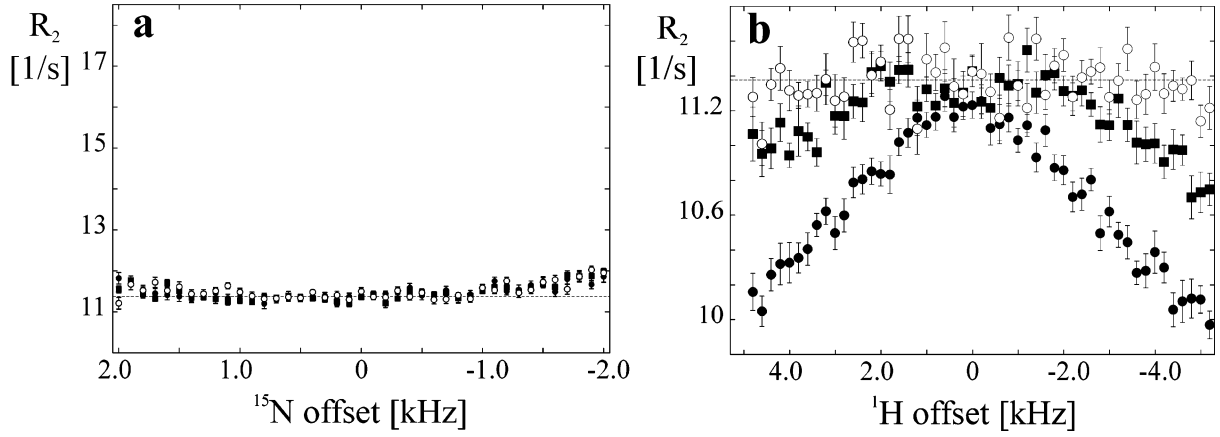

Figure 7. Experimentally derived transverse relaxation rates, R_2, of Trp41 $^{15}N^{\epsilon}$ from the spectrin SH3 domain. R_2 values were calculated from experimental ^{15}N $R_{1\rho}$ rates (1.17 kHz field) measured using ^{1}H CW decoupling (4.6 kHz field, a; 3.0 kHz, b) with phase x (solid circles), with phase alternated between x and $-x$ at equally spaced 10 ms intervals (solid squares) and with phase alternated randomly as described in the text, on average once per 10 ms (open circles). The dashed lines in the plots demark the R_2(CPMG) value obtained using a CPMG sequence with ^{15}N π pulses applied on-resonance. (a) ^{15}N R_2 vs ^{15}N offset from the spin-lock carrier measured with on-resonance ^{1}H CW fields. For comparative purposes the scale is the same as used in Figure 2. (b) ^{15}N R_2 vs ^{1}H offset from the carrier using an on-resonance ^{15}N spin-lock field.

duration with the phase of rf applied during each successive interval differing by 180°. The random phase alternation of rf employed here is an implementation of noise decoupling, proposed originally by Ernst,[48] with the average rate of phase alternation under experimental control. Thus, when phase alternations are described as occurring every 2 ms on average, for example, (see below) what is meant is that during a spin-lock interval of T ms $(T/2) - 1$ phase changes would occur, with the time between changes (denoted by d_i, in Figure 1d) randomly varying with each scan such that

$$\sum_{i=1}^{T/2} d_i = T \text{ ms}$$

As a first test we have performed simulations to compare the performance of on-resonance CW decoupling using a field of constant phase (Figure 6, red) with the ^{1}H decoupling scheme reported in Figure 1d (Figure 6, phase alternations every 2, 5, and 10 ms, on average, denoted by blue, green, and yellow curves respectively) using a homogeneous 2 kHz ^{15}N spin-lock field. Not surprising, efficient suppression of cross-correlation is achieved over a wide range of ^{15}N offsets in all cases. However, if the phase alternation is too fast (more than once every 5 ms) the simulated ^{15}N $R_{1\rho}$ values overestimate the correct values by several percentage points. In contrast, for rates on the order of once per 5−10 ms $R_{1\rho}$ values are essentially error-free.

Figure 7a shows ^{15}N R_2 values obtained from experimental $R_{1\rho}$ rates of the $^{15}N^{\epsilon}$ spin of Trp41 in the spectrin SH3 domain using a 4.6 kHz ^{1}H on-resonance CW decoupling field with constant phase (solid circles), with phase alternation by 180° every 10 ms (solid squares) and with random alternation of phase ($\pm x$, open circles) every 10 ms, on average. The dashed line indicates the R_2(CPMG) value. It is clear that all methods of proton decoupling are equally effective. In contrast, for off-resonance ^{1}H decoupling the performance of the constant phase CW field is poor for ^{1}H offset values greater than approximately 0.8 kHz (Figure 7b, 3 kHz field, solid circles) as is observed from the decrease in the measured relaxation rate due to the incomplete suppression of dipole−CSA cross-correlations. Systematic phase alternation of the CW field every 10 ms using the scheme of Figure 1c gives acceptable results over a bandwidth of ±2 kHz (solid squares). Better results are obtained, however, with random phase alternation every 10 ms, on average (bandwidth of ∼±3 kHz). We recommend, therefore, that this approach be employed on a per-transient basis. A formal analysis of the suppression of cross-correlation by random phase alternation of the ^{1}H CW decoupling field is presented in the Appendix. Briefly, the idea behind the approach is to suppress the transfer from in-phase (S_X) to anti-phase magnetization ($2S_XI_Z$) using a scheme which is sufficiently broadbanded so as to cover the range of amide ^{1}H offsets in a protein. The sequence used here effectively averages to zero ^{1}H magnetization (I_Z) at a rate that is fast compared to cross-correlated relaxation over a wide range of ^{1}H offsets so that the flow of magnetization from S_X to $2S_XI_Z$ due to cross-correlation is essentially canceled.

As a final check that randomly changing the phase of the ^{1}H CW decoupling field suppresses cross-correlation and does not introduce other systematic errors into the measurement of ^{15}N $R_{1\rho}$ values we have measured transverse relaxation rates for protein L using the scheme of Figure 1d. These values have been subsequently compared with those obtained with CPMG-based schemes.

Figure 8a shows a comparison of backbone ^{15}N R_2(CPMG) values with those obtained using the sequence of Figure 1a (applying ^{1}H π pulses every 4 ms). Note that the CPMG data has been corrected for off-resonance effects.[24] A systematic difference in the rates is obtained with the values measured in the spin-lock experiment on average higher by 7%. In contrast, an excellent correlation is noted between R_2(CPMG) and spin-lock R_2 values when the sequence of Figure 1d is employed, using a 4.5 kHz ^{1}H CW decoupling field, with random phase alternation every 10 ms, on average (Figure 8b).

An alternative strategy to suppress cross-correlation effects between dipolar and CSA relaxation mechanisms while at the same time avoiding the artifacts described in the present work is one in which ^{1}H pulses are applied only infrequently (see

(48) Ernst, R. R. *J. Chem. Phys.* **1966**, *45*, 3845−3861.

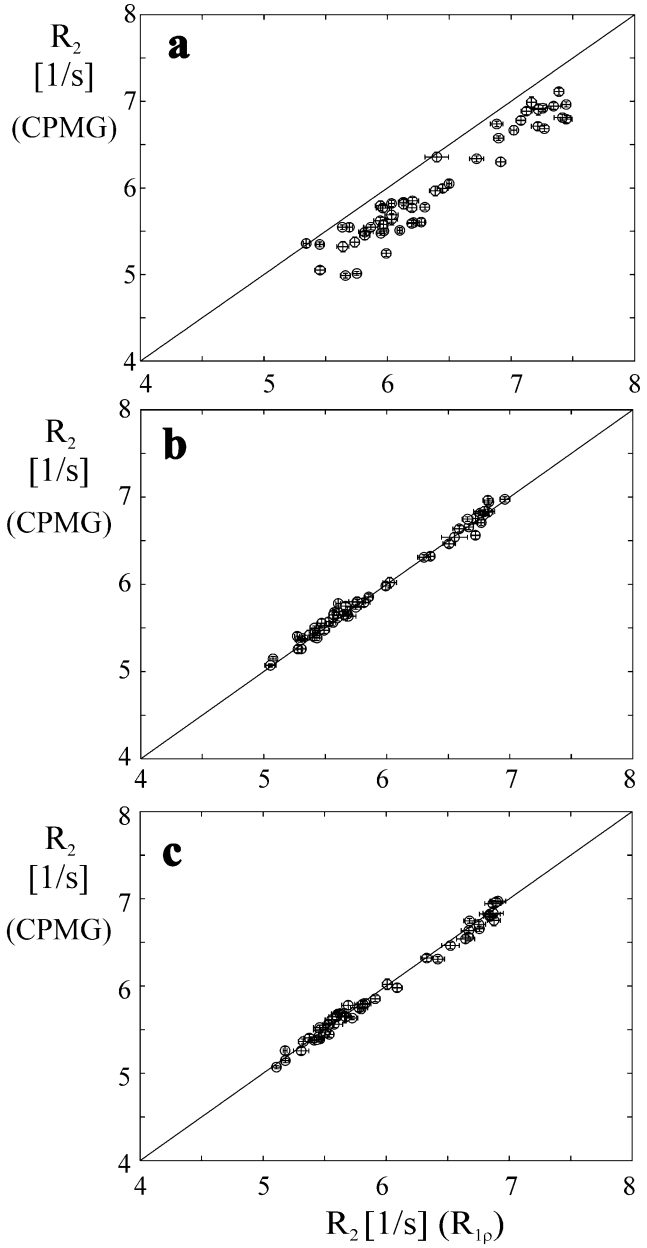

Figure 8. Experimental R_2 values of backbone ^{15}N spins in protein L. (a) R_2(CPMG) values after correction for off-resonance effects [24] vs R_2 rates obtained from $R_{1\rho}$ values, $R_2(R_{1\rho})$, measured using the scheme of Figure 1a with ^{1}H π pulses applied every 4.0 ms and a 1.6 kHz spin-lock field. (b) Correlation between R_2(CPMG) values (after correction for off-resonance effects) and $R_2(R_{1\rho})$ rates measured using a 4.5 kHz ^{1}H CW field with random phase alternation on average once per 10.0 ms (Figure 1d). (c) Correlation between R_2(CPMG) values and $R_2(R_{1\rho})$ rates measured with infrequent application of ^{1}H π pulses. In the present implementation $R_{1\rho}$ values were calculated from a series of nine ^{15}N spin-lock delays, T, extending to 120 ms. For $T < 40$ ms, 40 ms $\le T <$ 80 ms, 80 ms $\le T <$ 120 ms and $T = 120$ ms $k = 0$, 1, 2, or 3 pulses, respectively, were applied according to the scheme $(T/(2k)-\pi(^1\mathrm{H})-T/(2k))_{k,k\neq 0}$. In the CPMG scheme 92 μs ^{15}N π pulses were applied at 378 μs intervals.

Figure 2a and eq 6). Simulations establish that if spin-lock times extend up to $\tau \approx T_{1\rho}$, and that if three ^{1}H π pulses are applied during this interval, ^{15}N transverse relaxation rates are measured that exceed the correct value by less than 2%. We have implemented a scheme where for X spin-lock times, T, such that $0 \le T < \tau/3$, ^{1}H pulses are not applied, for $\tau/3 \le T < 2\tau/3$ a single π pulse is applied in the center of the spin-lock period, for $2\tau/3 \le T < \tau$ a pair of ^{1}H pulses are applied separated by $T/2$ (i.e., $[T/4-\pi(^1\mathrm{H})-T/4]_2$), while for $T = \tau$ 3 ^{1}H π pulses are inserted during the spin-lock (i.e., $[T/6-\pi(^1\mathrm{H})-T/6]_3$). Figure 8c shows the correlation between $R_2(R_{1\rho})$ values measured on protein L using this approach and R_2(CPMG) values, corrected for off-resonance effects.[24] An excellent correlation between R_2 values measured using these two methods is obtained as well.

Over the past decade a large number of NMR-based dynamics studies have made use of transverse relaxation rates obtained from $R_{1\rho}$ measurements. We have shown here that such values can be in error when either ^{1}H π pulses applied at regular short-spaced intervals or WALTZ16 decoupling fields are employed to suppress cross-correlation between X−H dipolar, X CSA relaxation interference. The errors can be minimized (less than ~5%) so long as spin-lock fields greater than 2 kHz and delays between ^{1}H π pulses in excess of 5 ms are employed. However, systematic errors can be reduced substantially beyond this level with new schemes which have been tested through both simulation and experiment. It is anticipated that these new methods will be important additions to experiments for measuring both ps−ns and slower μs−ms dynamics via on- and off-resonance spin relaxation, in particular in cases when a wide range of spin-lock fields are employed.[49]

Acknowledgment. This work was supported by grants from the Natural Sciences and Engineering Research Council of Canada and the Canadian Institutes of Health Research (CIHR). O.M and N.R.S. acknowledge funding from the Ministerio de Educacion y Cultura (MEC) and the CIHR, respectively. We thank Dr. R. Muhandiram for help with implementing the ^{1}H decoupling schemes. The pulse sequence code described is available upon request from the authors.

Appendix

The efficient suppression of ^{15}N−^{1}H dipolar−^{15}N CSA cross-correlation over a wide range of ^{1}H offsets by the application of a ^{1}H rf field with random phase alternations can be rationalized using the formalism developed by Griesinger and Ernst.[50] We start with eq 8 of their work which describes the time-dependent effective cross-relaxation rate between two normalized magnetization modes B_i and B_j

$$R_{ij}(t) = \frac{1}{t}\int_0^t Tr\{B_i^+(t')\hat{\Gamma}B_j(t')\}\,dt' \qquad \text{(A1)}$$

where $\hat{\Gamma}$ is the Redfield relaxation superoperator[39] and trajectories $B_i(t)$ and $B_j(t)$ are calculated neglecting relaxation as

$$B_i(t) = U(t)B_iU^{-1}(t),\ B_j(t) = U(t)B_jU^{-1}(t) \qquad \text{(A2)}$$

The unitary transformation $U(t)$, describing evolution of magnetization under (*i*) an rf field with phase randomly alternated from x to $-x$ applied to spin I and (*ii*) an off-resonance spin-lock field on spin S, is given by,

$$U(t) = U_I(t)U_S(t) \qquad \text{(A3)}$$

(49) Szyperski, T.; Luginbuhl, P.; Otting, G.; Guntert, P.; Wuthrich, K. *J. Biomol. NMR* **1993**, *3*, 151−164.
(50) Griesinger, C.; Ernst, R. R. *Chem. Phys. Lett.* **1988**, *152*, 239−247.

where

$$U_I(t) = \prod_{q=1}^{n} \exp[-i(\epsilon_q \nu_{1I} I_X + \Omega_I I_Z)\Delta t_q], \sum_{q=1}^{n} \Delta t_q = t \quad \text{(A4.1)}$$

$$U_S(t) = \exp[-i(\nu_{1S} S_X + \Omega_S S_Z)t] \quad \text{(A4.2)}$$

and ϵ_q is a factor alternating between 1 and -1 accounting for phase changes of the rf field applied on spin *I*.

Consider now the dipole−CSA cross-correlated cross-relaxation rate between $B_i = S'_Z$ and $B_j = 2S'_Z I_Z$ where S'_Z corresponds to spin-locked *S* magnetization, $S'_Z = S_X \sin\theta_S + S_Z \cos\theta_S$, $\theta_S = \text{arccot}(\Omega_S/\nu_{1S})$. Substituting B_i and B_j into eq A1 and making use of the fact that I_Z commutes with $U_S(t)$ and S'_Z commutes with $U_I(t)$ and $U_S(t)$ we obtain

$$R^{\text{DD-CSA}}(t) = Tr\left\{S'_Z \hat{\Gamma} 2S'_Z \left(\frac{1}{t}\int_0^t U_I(t') I_Z U_I^{-1}(t')\mathrm{d}t'\right)\right\} \quad \text{(A5)}$$

Focusing on the integral in eq A5 we note that it can be represented as a linear combination

$$\frac{1}{t}\int_0^t U_I(t') I_Z U_I^{-1}(t')\mathrm{d}t' = \chi_X(t) I_X + \chi_Y(t) I_Y + \chi_Z(t) I_Z \quad \text{(A6)}$$

where

$$\chi_q(t) = \frac{1}{t} Tr\{I_q \int_0^t U_I(t') I_Z U_I^{-1}(t')\mathrm{d}t'\} / Tr\{I_q^2\}\ ,\ q = x,y,z \quad \text{(A7)}$$

Substituting eq A6 into eq A5 we obtain

$$R^{\text{DD-CSA}}(t) = \sum_{q=x,y,z} \chi_q(t) Tr\{S'_Z \hat{\Gamma} 2S'_Z I_q\} \quad \text{(A8)}$$

Goldman has shown[51] that in the case of dipole−CSA cross-correlated relaxation $Tr\{S'_Z \hat{\Gamma} 2S'_Z I_q\} = 0$ for $q = x,y$ leading finally to

$$R^{\text{DD-CSA}}(t) = \chi_Z(t) Tr\{S'_Z \hat{\Gamma} 2S'_Z I_Z\} \quad \text{(A9)}$$

The factor $\chi_Z(t)$ can be viewed as an attenuation coefficient that characterizes the efficiency of the proposed decoupling scheme for suppression of dipole−CSA cross-correlations. The period of time *t* over which the integration is performed in eqs A5−7 is chosen such that it is short on the time scale of cross-relaxation but much longer than the average interval Δt_q in eq A4 corresponding to a period of constant ^{1}H rf phase. Under these conditions the effective cross-relaxation rate defined by eq A9 becomes essentially time-independent, $\chi_Z(t) \cong \chi_Z$, $R^{\text{DD-CSA}}(t) \cong R^{\text{DD-CSA}}$.

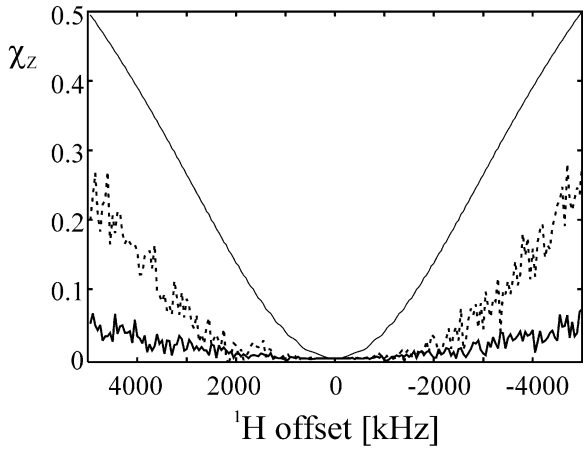

Figure 9. Attenuation factor χ_Z (see Appendix) versus ^{1}H offset, illustrating averaging of ^{1}H *Z*-magnetization under the action of a 5.0 kHz ^{1}H rf field with constant phase (t = 20 ms, thin solid line), with random phase alternation between x and $-x$, on average at intervals of 10 ms (t = 20 ms, dashed line; t = 100 ms, bold solid line) (see Appendix for details).

The attenuation coefficient χ_Z in eq A9 represents the average *z*-projection of the magnetization vector **I** over the trajectory sampled during the ^{1}H decoupling scheme with randomly alternated phase. Figure 9 shows values of χ_Z as a function of ^{1}H offset for a 5 kHz CW rf field with no phase alternation after a period of 20 ms (thin solid line) and for a 5 kHz field with the phase alternated between $+x$ and $-x$, on average every 10 ms, after 20 ms (i.e., one phase change; dashed line) and after 100 ms (i.e., nine phase changes; bold solid line). χ_Z values shown are averages over 100 realizations (i.e., are computed from 100 trajectories with random phase switching). Note that the number of phase changes increases with the length of the relaxation delay, leading to improved suppression of cross-correlated spin-relaxation. This is important since, unless suppressed, the effects of cross-correlation become more pronounced with increased relaxation delays. Figure 9 shows that for a spin-lock time of 100 ms χ_Z values are close to zero for ^{1}H offsets less than $\pm$1.5 kHz, leading to very efficient suppression of cross-correlation. Excellent suppression has been observed experimentally, as illustrated in Figure 7b.

JA0204776

(51) Goldman, M. *J. Magn. Reson.* **1984**, *60*, 437−452.
(52) Marion, D.; Ikura, M.; Tschudin, R.; Bax, A. *J. Magn. Reson.* **1989**, *85*, 393−399.
(53) Kay, L. E.; Keifer, P.; Saarinen, T. *J. Am. Chem. Soc.* **1992**, *114*, 10663−10665.
(54) Schleucher, J.; Sattler, M.; Griesinger, C. *Angew. Chem., Int. Ed. Engl.* **1993**, *32*, 1489−1491.